Solution of the Electric Field Integral Equation When It Breaks Down

Jianfang Zhu, Saad Omar, *Student Member, IEEE*, and Dan Jiao, *Senior Member, IEEE*

***Abstract*—With a method developed in this work, we find the solution of the original electric field integral equation (EFIE) at an arbitrary frequency where the EFIE breaks down due to low frequencies and/or dense discretizations. This solution is equally rigorous at frequencies where the EFIE does not break down and is independent of the basis functions used. We also demonstrate, both theoretically and numerically, the fact that although the problem is commonly termed *low-frequency* breakdown, the solution at the EFIE breakdown can be dominated by *fullwave* effects instead of just static or quasi-static physics. The accuracy and efficiency of the proposed method is demonstrated by numerical experiments involving inductance, capacitance, RCS extraction, and a multi-scale example with a seven-orders-of-magnitude ratio in geometrical scales, at all breakdown frequencies of an EFIE. In addition to the EFIE, the proposed method is also applicable to other integral equations and numerical methods for solving Maxwell's equations.**

***Index Terms*—Dense discretization breakdown, electric field integral equation, electromagnetic analysis, full-wave analysis, low-frequency breakdown, scattering.**

I. Introduction

EVER since the numerical methods were introduced for electromagnetic (EM) analysis, researchers observed the breakdown of a full-wave solution of Maxwell's equations at low frequencies [1]–[3]. The term "breakdown" refers to a phenomenon that a numerical system becomes singular, preventing even a direct solution. This problem is important and becoming even more critical in today's engineering problems analyzed via EM simulators. As an example, in digital, analog, and mixed-signal integrated circuit design where signals have a wide bandwidth from zero to about the third harmonic frequency, the breakdown frequency of full-wave solvers (typically around tens of MHz) falls right within the range of circuit operating frequencies. The breakdown due to dense discretizations has also been observed and studied [4]–[8]. The dense discretizations cannot be avoided in problems with fine features relative to working wavelength. Although for this case, apparently the breakdown is caused by dense discretizations, the frequencies at which a full-wave solver breaks down are still lower than those frequencies where it does not break down.

Manuscript received May 06, 2013; revised April 03, 2014; accepted May 01, 2014. Date of publication May 09, 2014; date of current version July 31, 2014. This work was supported by a grant from Intel Corporation, a grant from the Office of Naval Research under Award N00014-10-1-0482, and a grant from the National Science Foundation under Award 0747578.

The authors are with the School of Electrical and Computer Engineering, Purdue University, West Lafayette, IN 47907 USA (e-mail: djiao@purdue.edu).

Color versions of one or more of the figures in this paper are available online at http://ieeexplore.ieee.org.

Digital Object Identifier 10.1109/TAP.2014.2322899

Existing approaches for overcoming the low-frequency breakdown problem can be categorized into two classes. One class is to stitch a static- or quasi-static based electromagnetic solver with a full-wave based electromagnetic solver. The accuracy of this approach is questionable because static/quasi-static solvers involve fundamental approximations such as decoupled $\mathbf{E}$ and $\mathbf{H}$. In addition, at which frequency the switching between different solvers has to be done is an issue. In practice, engineers often have to employ an approximation based model to achieve a smooth transition between static, quasi-static, and full-wave solvers, which introduces another level of inaccuracy. Moreover, this approach is built on an underlying assumption that there exists no such frequency, where the static and/or quasi-static approximations are not valid and the fullwave solvers still break down. The validity of this assumption needs to be assessed for different applications.

The other class of methods for solving the low-frequency breakdown problem is to extend the validity of full-wave solvers to low frequencies. In integral equation solvers, the loop-tree and loop-star basis function based methods separate the current into a divergence-free current and a non-divergence-free current [1], [2], [9]–[11]. The decoupling (or weak coupling) between the two currents at low frequencies is utilized to construct a better conditioned numerical system to solve when the EFIE breaks down. The current-charge integral equation [12], [13] and the augmented electric field integral equation [14], [15] introduce charges as additional unknowns. The decoupling (or weak coupling) between the current and the charge is utilized to overcome the low-frequency breakdown. The current solved from these methods, at low frequencies, is only a divergence-free current. Similar to the first class of methods, when the EFIE breaks down, whether the divergence-free current is decoupled from the non-divergence-free current, and whether the current is decoupled from the charge need to be examined for different applications. There also exist preconditioned EFIE methods for addressing the low-frequency breakdown problem such as Calderón preconditioner (CP) based methods [5]–[8], [16]. They have successfully improved the conditioning of the EFIE operator, and greatly reduced the number of iterations required by an iterative solver when the EFIE is ill-conditioned. However, at low frequencies, the original EFIE system matrix, numerically, becomes singular when the contribution from the vector potential is lost due to finite machine precision. No matter how good the preconditioner is, a singular matrix remains singular. To overcome this problem, existing preconditioned EFIE methods still rely on loop-star decomposition, thus switching to a different system of equations to solve at low frequencies rather than solving the original Rao–Wilton–Glisson (RWG)-

based system of equations. Take the Calderón preconditioner as an example, let $\mathcal{T}$ denote the EFIE operator. Although $\mathcal{T}^2$does not break down at low frequencies, a frequency-dependent term is lost in $\mathcal{T}^2$, and the singular $\mathcal{T}$ is also involved in the right-hand side of the system of equations. The static limit of the CP-EFIE is shown to yield a current that does not depend on frequency at low frequencies [6], which is different from the true solution of the original EFIE (this solution will be presented in this paper). The same holds true for the magnetic field IE (MFIE). Although it is well-conditioned, once the frequency-dependent terms are lost at low frequencies, the MFIE solution becomes inaccurate, although it does not break down.

One common characteristic shared by the second class of methods is that they all have changed the original EFIE system of equations, resulting from the traditional MoM-based solution with the RWG basis functions, to a new system of equations that is better conditioned to solve when the EFIE breaks down. This approach has its obvious advantage that a better-conditioned numerical system facilitates fast large-scale solutions. However, the solution to the original RWG-based EFIE, which has been widely used to solve electromagnetic problems and is theoretically valid from low to high frequencies, is still unknown when the EFIE breaks down. The root cause of the low-frequency breakdown is finite machine precision, which has been recognized by many papers on this topic. Once the breakdown occurs, apparently, the only way forward is to change the EFIE system to a different one that is solvable.

The contribution of this work is that we are able to overcome the barrier imposed by the finite machine precision, and successfully find the solution to the original full-wave EFIE system of equations from an arbitrarily high electrodynamic frequency all the way down to zero frequency. Different from existing methods that tackle the low-frequency breakdown from the perspective of how to change the original matrix, we derive a closed-form expression of the EFIE system matrix inverse at any frequency. By doing so, we avoid the breakdown caused by numerically solving the original system matrix. The closed-form expression of the EFIE inverse is rigorously derived from the eigenvectors and eigenvalues of a generalized eigenvalue problem governing the EFIE. This generalized eigenvalue problem can be solved at an arbitrarily low frequency including dc without breakdown. The proposed closed-form expression also demonstrates that the EFIE solution at breakdown can be a full-wave solution for which the divergence-free and non-divergence free currents, as well as the currents and the charges, are strongly coupled, and the static/quasi-static assumptions are invalid. This is especially true for multiscale problems that span more than six orders of magnitude in the ratio of geometrical scales. Such a phenomenon has not been reported in open literature. The existing literature on dense discretization breakdown and multiscale simulations reports cases where the aspect ratio of electric sizes is less than five orders of magnitude. For such an aspect ratio, the EFIE solution at breakdown is still dominated by static effects, which will become clear in the sequel.

In addition to the breakdown caused by the loss of the vector potential in the EFIE system matrix, we have also found the breakdown due to the loss of the frequency dependence of the right-hand side in scattering analysis, and the breakdown caused by the same loss in Green's function for scattered field computation. These two problems have been identified before [3], [9], [19] and termed as numerical cancellation problems. If the two breakdown issues are not resolved, the EFIE breakdown cannot be completely eliminated. We hence developed an analytical method to remove these two breakdown problems. This analytical method, again, is valid at any frequency.

Moreover, the proposed closed-form model of the EFIE's inverse explicitly reveals the frequency dependence of the EFIE solution when the EFIE solution at breakdown is dominated by static effects. Based on this frequency dependence, with negligible cost, one can find the solution of the EFIE when it breaks down from a single solution obtained at one non-breakdown frequency. For the case where the EFIE solution at breakdown is dominated by full-wave effects, one can use the solutions obtained from the traditional EFIE solver at a few non-breakdown frequencies to synthesize the EFIE solution at breakdown, by a fast method developed in this paper based on the essential idea of the proposed rigorous method. In this way, we equally bypass the barrier of finite machine precision; preserve the theoretical rigor of the proposed solution; while obtaining the EFIE solution when it breaks down without the need for solving the original governing eigenvalue problem.

The proposed method is a generic method for solving Maxwell equations based linear systems of equations composed of ω^2, ω, and constant terms, where ω denotes an angular frequency. Besides the EFIE, the method can be applied to other integral equations and numerical methods such as the finite element method [17], [18]. In addition to the RWG bases and Galerkin's schemes, the proposed method is also applicable to other basis functions and discretization methods.

II. Low-Frequency Breakdown Problem of the EFIE

A. MoM Solution of the EFIE

Consider a perfect electrically conducting object immersed in a medium with permittivity ε and permeability μ. The object is excited by an impressed source $\mathbf{E}_i$ that induces current $\mathbf{J}$ on the conducting surface. The source $\mathbf{E}_i$ can be a delta-gap voltage source commonly used for analyzing radiation and circuit problems; it can also be an incident field employed for scattering analysis. The current $\mathbf{J}$ satisfies the following electric field integral equation:

$$\hat{n}\times\mathbf{E}_i=\hat{n}\times\left\{\iint_S\left[j\omega\mu\mathbf{J}(\mathbf{r}')G(\mathbf{r},\mathbf{r}')+\frac{j}{\omega\varepsilon}\nabla'\cdot\mathbf{J}(\mathbf{r}')\nabla G(\mathbf{r},\mathbf{r}')\right]dS\right\} \quad (1)$$

in which $\mathbf{r}$ and $\mathbf{r}'$ are, respectively, observation and source points on the conducting surface, $\hat{n}$ is a unit vector normal to conducting surface, and G is dynamic Green's function

$$G(\mathbf{r},\mathbf{r}')=\frac{e^{-jk|\mathbf{r}-\mathbf{r}'|}}{4\pi|\mathbf{r}-\mathbf{r}'|} \quad (2)$$

where k is the wavenumber $\omega\sqrt{\mu\varepsilon}$.

By expanding the unknown surface current density $\mathbf{J}$ using RWG basis functions [20], and applying Galerkin's method to (1), we obtain the following linear system of equations:

$$\mathbf{Z}(\omega)I(\omega)=V(\omega) \quad (3)$$

where the system matrix $\mathbf{Z}$ is

$$\mathbf{Z}(\omega) = \frac{1}{j\omega}\mathbf{\Phi}(\omega) + j\omega\mathbf{A}(\omega) \tag{4}$$

in which $\mathbf{A}$ and $\mathbf{\Phi}$ are frequency dependent, the elements of which are given by

$$\begin{aligned}\mathbf{A}_{mn} &= \iint_{S_m} dS \iint_{S_n} [\mu \mathbf{J}_m(\mathbf{r}) \cdot \mathbf{J}_n(\mathbf{r}') G(\mathbf{r}, \mathbf{r}')] dS' \\ \mathbf{\Phi}_{mn} &= \iint_{S_m} dS \iint_{S_n} \left[\frac{1}{\varepsilon} \nabla \cdot \mathbf{J}_m(\mathbf{r}) \nabla' \cdot \mathbf{J}_n(\mathbf{r}') G(\mathbf{r}, \mathbf{r}')\right] dS'\end{aligned} \tag{5}$$

with $\mathbf{J}_m(\mathbf{J}_n)$ being the vector basis used to expand unknown current $\mathbf{J}$. The right-hand side of (3) has the following entries:

$$V_m = \iint_{S_m} \mathbf{J}_m(\mathbf{r}) \cdot \mathbf{E}_i(\mathbf{r}) dS. \tag{6}$$

As can be seen from (4), matrix $\mathbf{Z}$ is composed of two matrices $\mathbf{\Phi}$ and $\mathbf{A}$, each of which is associated with a different frequency dependence. A careful examination of the matrix properties of $\mathbf{\Phi}$ and $\mathbf{A}$ reveals that $\mathbf{A}$ is a full-rank matrix while $\mathbf{\Phi}$ is rank deficient. The deficiency of rank in $\mathbf{\Phi}$ is due to the nullspace of the divergence operator. Specifically, any solenoidal vector $\mathbf{J}$ satisfying $\nabla \cdot \mathbf{J} = 0$ would satisfy $\mathbf{\Phi} J = 0$. Therefore, $\mathbf{\Phi}$ is a singular matrix.

B. Analysis of the Low-Frequency Breakdown Problem

To analyze the breakdown problem of (3), consider the ratio of $j\omega\mathbf{A}_{mn}$ to $\mathbf{\Phi}_{mn}/(j\omega)$ in (4). It is proportional to the square of the electrical size of l,

$$|j\omega\mathbf{A}_{mn}|/|\mathbf{\Phi}_{mn}/(j\omega)| = O(k^2 l^2) \tag{7}$$

where l is proportional to the length of the mth edge in a space discretization. As an example, for state-of-the-art integrated circuits with μm-level geometrical dimensions, at and below tens of MHz, $j\omega\mathbf{A}_{mn}$ is 16 orders of magnitude smaller than $\mathbf{\Phi}_{mn}/(j\omega)$. Even if one uses double-precision computing, $\mathbf{A}$ is essentially treated as zero by computers when performing the addition of $j\omega\mathbf{A}$ and $\mathbf{\Phi}/(j\omega)$ in (4). As a result, the solution of (3) breaks down. Furthermore, if a structure involves fine discretizations relative to working wavelength such that the electric size square of the finest mesh size is smaller than machine precision, the EFIE also breaks down.

Based on (7), apparently, when the EFIE breaks down, the electric size of the problem is small since $k^2 l^2 < \delta$, where δ denotes machine precision. This leads to the belief that the EFIE solution at breakdown must be a static solution, and thus using a static solution or incorporating static physics seems to be an accurate way to solve the low-frequency breakdown problem. However, as can be seen from (7), different feature sizes l have different electrical sizes. Consequently, they break down at different frequencies. When a highly multiscaled structure is considered due to either dense discretization or the nature of the problem, the breakdown starts to occur at a frequency where (7) is less than machine precision for the smallest feature size. However, at this frequency, the electrical size of the largest dimension can still be comparable to wavelength, thus requiring a full-wave analysis. In other words, although the problem is termed *low-frequency* breakdown, this does not mean the EFIE solution at breakdown must be a static/quasi-static solution. Completely or partially decoupling $\mathbf{E}$ from $\mathbf{H}$ or introducing other static/quasi-static approximations may yield incorrect results.

III. Proposed Method

During the study of the low-frequency breakdown of the EFIE, we found that one can encounter three types of breakdown phenomena. If any one of these three breakdown problems is not properly addressed, the EFIE breakdown cannot be completely solved. The first breakdown is due to the loss of the vector potential term in the EFIE system matrix at low frequencies; the second breakdown is caused by the loss of the frequency dependence of the right-hand side vector such as an incident field used in scattering analysis; and the third breakdown occurs when evaluating the scattered field or RCS at low frequencies. In the following three subsections, we show how each breakdown is overcome in this work.

A. Analytical Derivation of the EFIE System Matrix Inverse

Based on our work in [17], [18], [26], the solution of (3) resulting from the discretization of the EFIE is governed by the following generalized eigenvalue problem:

$$\mathbf{\Phi}(\omega)x(\omega) = \lambda(\omega)\mathbf{A}(\omega)x(\omega) \tag{8}$$

where $\mathbf{\Phi}$ and $\mathbf{A}$ are the same as those in (5), λ is the frequency-dependent eigenvalue, and x is the corresponding frequency-dependent eigenvector. Since $\mathbf{A}$ and $\mathbf{\Phi}$ are nondefective, the eigenvalues λ are finite numbers, including zeros due to the nullspace of $\mathbf{\Phi}$. The square root of the eigenvalue λ represents the **complex** resonance frequency of the structure at the angular frequency ω, the largest modulus of which is inversely proportional to the smallest mesh size, while the smallest nonzero modulus is inversely proportional to the largest physical dimension of the structure being simulated. The eigenvectors x are linearly independent of each other [21]. Different from the system matrices resulting from a finite element based analysis, $\mathbf{\Phi}$ and $\mathbf{A}$ are both complex valued and frequency dependent due to the inherent presence of Green's function in IE based formulations. Therefore, the generalized eigenvalue problem shown in (8) is frequency dependent. Only at low frequencies, where $e^{-jk|\mathbf{r}-\mathbf{r}'|}$ in (2) can be approximated as 1, $\mathbf{\Phi}$ and $\mathbf{A}$ can be considered real, and (8) becomes frequency independent.

Define the eigenvalues of (8) by $\lambda_1, \lambda_2, \ldots, \lambda_N$ and the corresponding eigenvectors by $x_1, x_2, \ldots, x_N$. Let $\mathbf{W}$ be the matrix whose column vectors are eigenvectors

$$\mathbf{W} = [x_1, x_2, \ldots, x_N] \tag{9}$$

and Λ be the diagonal matrix of eigenvalues

$$\Lambda = \begin{bmatrix} \lambda_1 & & \\ & \ddots & \\ & & \lambda_N \end{bmatrix}. \tag{10}$$

Since $\mathbf{W}$ is full rank, its column vectors constitute a complete set of bases in an N dimensional space. Thus, we can use $\mathbf{W}$ to expand the unknown current vector I in (3). We thereby obtain

$$I = \mathbf{W}\tilde{I} \tag{11}$$

in which $\tilde{I}$ is the unknown coefficient vector to be solved. Substituting (11) into (3), and multiplying (3) by $\mathbf{W}^T$ on both sides, we obtain

$$\left(\frac{1}{j\omega}\tilde{\mathbf{\Phi}} + j\omega\tilde{\mathbf{A}}\right)\tilde{I} = \tilde{V} \tag{12}$$

where

$$\tilde{\mathbf{\Phi}} = \mathbf{W}^T\mathbf{\Phi}\mathbf{W} \qquad \tilde{\mathbf{A}} = \mathbf{W}^T\mathbf{A}\mathbf{W} \tag{13}$$

$$\tilde{V} = \mathbf{W}^T V. \tag{14}$$

Since $\mathbf{W}$ is the eigenvector matrix, and Λ is the eigenvalue matrix, from (8), we have

$$\mathbf{\Phi}\mathbf{W} = \mathbf{A}\mathbf{W}\mathbf{\Lambda}. \tag{15}$$

Multiplying both sides by $\mathbf{W^T}$, we obtain

$$\mathbf{W}^T\mathbf{\Phi}\mathbf{W} = \mathbf{W}^T\mathbf{A}\mathbf{W}\mathbf{\Lambda}. \tag{16}$$

From this and (13) we find

$$\tilde{\mathbf{\Phi}} = \tilde{\mathbf{A}}\mathbf{\Lambda}. \tag{17}$$

Substituting (17) into (12) we have

$$\begin{pmatrix} \frac{\lambda_1-\omega^2}{j\omega} & & \\ & \ddots & \\ & & \frac{\lambda_N-\omega^2}{j\omega} \end{pmatrix}\tilde{I} = \tilde{\mathbf{A}}^{-1}\tilde{V}. \tag{18}$$

Thus, the unknown coefficient vector $\tilde{I}$ can be found by solving a diagonal system (18), from which the original solution I can be obtained using (11). The above derivation is for one right-hand side V in (3). If the right-hand side V is an identity matrix $\mathbf{I}$, we obtain the inverse of $\mathbf{Z}$ at an arbitrary ω, which is

$$\mathbf{Z}(\omega)^{-1} = j\omega\mathbf{W}(\omega)(\mathbf{\Lambda}(\omega) - \omega^2\mathbf{I})^{-1} \times (\mathbf{W}^T\mathbf{A}\mathbf{W})^{-1}\mathbf{W}(\omega)^T, \quad \forall\omega. \tag{19}$$

In the above, by analytically deriving the inverse of the EFIE-based system matrix $\mathbf{Z}$, we avoid the breakdown caused by the loss of the vector potential term when numerically solving $\mathbf{Z}$. However, the inverse shown in (19) can still break down at low frequencies if the inexact zero eigenvalues of (8) are not fixed to be exact zero. To explain, the eigenvalues of (8) can be divided into two groups: one group is associated with the nullspace of $\mathbf{\Phi}$, and the other is associated with the nonzero complex resonance frequencies of the structure at the given frequency. The first group has zero eigenvalues. But numerically, they cannot be computed as exact zeros. Instead, they can be computed as very large numbers. For example, in a typical on-chip circuit having μm-level dimensions, the largest eigenvalue of (8) can be as large as 10^{32} (rad/s)^2 while the zero eigenvalues are numerically obtained as 10^{16} (rad/s)^2. This is because in general, eigenvalue solvers first converge to the largest eigenvalue of the numerical system, the eigenvalues that are 16 orders of magnitude smaller than the largest one are not distinguishable in double-precision computing. Even though these inexact zero eigenvalues do not induce much error at high frequencies, they lead to a completely wrong frequency dependence of the EFIE solution at low frequencies. A natural remedy to this problem is to fix the inexact zero eigenvalues to be exact zeros. Since in magnitude, zero eigenvalues are the smallest eigenvalues of (8) and there is a clear gap between the zero eigenvalue and the first nonzero eigenvalue as the structure being simulated is finite, the zero eigenvalues can be readily identified and their inaccuracy can be analytically fixed.

With the inexact zero eigenvalues fixed to be exact zeros, (19) becomes (20), shown at the bottom of the page (the argument ω is omitted for simplicity), where $\mathbf{W}_0$ and $\mathbf{W}_h$, respectively, represent the eigenvectors of (8) corresponding to zero and nonzero eigenvalues; $\mathbf{W}$ is the union of $\mathbf{W}_0$ and $\mathbf{W}_h$, i.e., $\mathbf{W} = [\mathbf{W}_0\ \mathbf{W}_h]$; Λ_h is the diagonal matrix of nonzero eigenvalues, and the $[(\mathbf{W}^T\mathbf{A}\mathbf{W})^{-1}\mathbf{W}^T]_o$ represents the upper block of matrix $(\mathbf{W}^T\mathbf{A}\mathbf{W})^{-1}\mathbf{W}^T$. The number of rows in $[(\mathbf{W}^T\mathbf{A}\mathbf{W})^{-1}\mathbf{W}^T]_o$ is the same as the number of columns in $\mathbf{W}_0$. The $[(\mathbf{W}^T\mathbf{A}\mathbf{W})^{-1}\mathbf{W}^T]_h$ is the remaining block of $(\mathbf{W}^T\mathbf{A}\mathbf{W})^{-1}\mathbf{W}^T$. The$\mathbf{W}_0$ in (20) is the nullspace of $\mathbf{\Phi}$ since it corresponds to the zero eigenvalues of (8), and thus satisfies

$$\mathbf{\Phi}\mathbf{W}_0 = 0. \tag{21}$$

In what follows, for convenience, we will refer to $\mathbf{W}_0$ as the dc eigenmodes while $\mathbf{W}_h$ as the higher order eigenmodes since the former corresponds to a zero resonance frequency, whereas the latter has eigenvalues whose magnitude is higher.

It is worth mentioning that (20) is not a singular value decomposition (SVD) of the EFIE inverse since $\mathbf{W}$ is not unitary. In fact, the SVD cannot solve the EFIE breakdown problem. To explain this, if one takes the SVD of $\mathbf{Z}$ directly, when $\mathbf{Z}$ is singular so is its SVD. Since the singular values are frequency dependent and their behavior is not analytically known, it is not feasible to analytically correct wrong singular values to obtain a correct inverse. In addition, it can be seen that the proposed approach is valid regardless of whether the system matrices in (4) are generated from RWG bases or other bases, from Galerkin's schemes or other schemes. The essential idea can also be applied to other integral equation solvers and partial differential equation based ones. Furthermore, the proposed method is not restricted to the homogeneous materials. For inhomogeneous materials that can be conveniently analyzed by the volume IE or finite element methods, the proposed method is equally applicable.

$$\mathbf{Z}(\omega)^{-1} = j\omega\left[\mathbf{W}_0\ \mathbf{W}_h\right]\begin{bmatrix} 0-\omega^2\mathbf{I} & 0 \\ 0 & \Lambda_h-\omega^2\mathbf{I} \end{bmatrix}^{-1}(\mathbf{W}^T\mathbf{A}\mathbf{W})^{-1}\mathbf{W}^T = \frac{1}{j\omega}\mathbf{W}_0\left[(\mathbf{W}^T\mathbf{A}\mathbf{W})^{-1}\mathbf{W}^T\right]_o + j\omega\mathbf{W}_h(\Lambda_h-\omega^2\mathbf{I})^{-1}\left[(\mathbf{W}^T\mathbf{A}\mathbf{W})^{-1}\mathbf{W}^T\right]_h, \forall\omega \tag{20}$$

The inverse of the EFIE-based system matrix derived in (20) is rigorous from electrodynamic frequencies all the way down to zero frequency. It does not suffer from low-frequency breakdown. This is because given an arbitrary frequency ω including zero, $\mathbf{W}_0$, $\mathbf{W}_h$, and Λ_h in (20) can be accurately found from (8) without breakdown. Since $\mathbf{W}$ is full rank and $\mathbf{A}$ is invertible, $(\mathbf{W}^T\mathbf{A}\mathbf{W})^{-1}$ in (20) can also be obtained at any frequency. At dc, the first term in (20) is singular for a right-hand side that is constant, which, in fact, agrees with the theoretical result. This is because for a constant voltage excitation, a perfectly conducting loop structure modeled by the EFIE behaves as an ideal inductor at low frequencies. In addition, it becomes a short circuit at zero frequency and its impedance becomes zero. Thus, the current tends to infinity as the excitation voltage is maintained at a constant level and this agrees with the result shown in (20). For an incident-field based excitation, the first term in (20) is not singular because the $j\omega$ in the denominator will be canceled by the $j\omega$ factor present in the excitation, which will be discussed in more detail in the following Section III-B.1.

At low frequencies where $\mathbf{A}$ and $\mathbf{\Phi}$ become real, let $\mathbf{A}$ be denoted by $\mathbf{A_0}$, and $\mathbf{\Phi}$ by $\mathbf{\Phi_0}$. Since $\mathbf{A_0}$ is positive definite, $\Phi_\mathbf{0}$ is semipositive definite, (8) is said to be a symmetric positive definite generalized eigenvalue problem [22, pp. 231–240]. For this class of problem, the eigenvectors are both Φ- and $\mathbf{A}$-orthogonal. Hence, we have

$$\mathbf{W}^T\mathbf{A}_0\mathbf{W} = \mathbf{I},\ \mathbf{W}^T\mathbf{\Phi}_0\mathbf{W} = \mathbf{\Lambda}. \tag{22}$$

Thus, (20) can be reduced to

$$\mathbf{Z}(\omega)^{-1} = \frac{1}{j\omega}\mathbf{W}_0\mathbf{W}_0^T + j\omega\mathbf{W}_h(\Lambda_h - \omega^2\mathbf{I})^{-1}\mathbf{W}_h^T. \tag{23}$$

When ω^2 compared to Λ_h is negligible, it can be further reduced to

$$\mathbf{Z}(\omega)^{-1} = \frac{1}{j\omega}\mathbf{W}_0\mathbf{W}_0^T + j\omega\mathbf{W}_h(\Lambda_h)^{-1}\mathbf{W}_h^T. \tag{24}$$

B. Solution to the EFIE at an Arbitrary Frequency

Based on (20), the solution of the EFIE at an arbitrary ω can be written as

$$\begin{aligned} I(\omega) &= \mathbf{Z}(\omega)^{-1}V \\ &= \frac{1}{j\omega}\mathbf{W}_0\left[(\mathbf{W}^T\mathbf{A}\mathbf{W})^{-1}\mathbf{W}^T\right]_o V \\ &\quad + j\omega\mathbf{W}_h(\Lambda_h - \omega^2\mathbf{I})^{-1}\left[(\mathbf{W}^T\mathbf{A}\mathbf{W})^{-1}\mathbf{W}^T\right]_h V(\forall\omega). \end{aligned} \tag{25}$$

Since $\mathbf{W}_0$ is the nullspace of $\mathbf{\Phi}$, whose eigenvectors are divergence free, we can readily identify the divergence-free component I_0 and the non-divergence-free component I_h from (25) as follows:

$$\begin{aligned} I(\omega) &= I_0(\omega) + I_h(\omega), \quad (\forall\omega) \\ I_0 &= \frac{1}{j\omega}\mathbf{W}_0\left[(\mathbf{W}^T\mathbf{A}\mathbf{W})^{-1}\mathbf{W}^T\right]_o V, \\ I_h &= j\omega\mathbf{W}_h(\Lambda_h - \omega^2\mathbf{I})^{-1}[(\mathbf{W}^T\mathbf{A}\mathbf{W})^{-1}\mathbf{W}^T]_h V. \end{aligned} \tag{26}$$

The above appears to be a separation (decoupling) of the divergence-free and non-divergence-free currents. This is not true. As shown in (26), although a current can be decomposed into I_0 and I_h at any frequency, the two are *coupled* as indicated by the $(\mathbf{W}^T\ \mathbf{A}\mathbf{W})^{-1}$ term, which is not identity but a densely populated matrix. Both I_0 and I_h have a complicated frequency dependence. I_0 is determined by not only $\mathbf{W}_0$ but also $\mathbf{W}_h$, and the same is true for I_h. Furthermore, for higher frequencies, the contribution from I_0 even becomes negligible as compared to that from I_h, which explains why quasi-Helmholtz decomposition is not effective at high frequencies. Only when frequency is low that (8) becomes real, and thereby $(\mathbf{W}^T\mathbf{A}\mathbf{W})^{-1}$ becomes an identity matrix, the two currents can be considered decoupled, i.e., independent of each other. In this case, we can obtain their expressions from (26) as the following:

$$I_0 = \frac{1}{j\omega}\mathbf{W}_0\mathbf{W}_0^T V \tag{27}$$

$$I_h = j\omega\mathbf{W}_h(\Lambda_h - \omega^2\mathbf{I})^{-1}\mathbf{W}_h^T V. \tag{28}$$

1) Solution to the Plane Wave Incidence in Scattering Analysis: In scattering analysis, V in (3) is related to an incident field. The specific form considered in this paper is $\mathbf{E}_i = \hat{E}_0 e^{-j\mathbf{k}\cdot\mathbf{r}}$, which represents a generic plane wave polarized in $\hat{E}_0$ direction. Such an incident field is frequency dependent. However, at low frequencies, it becomes a constant with respect to frequency in a computer simulation when the phase of the incident field is too small to be captured by the finite machine precision. As a result, I_0 shown in (26) and (27), which is the divergence-free current, becomes inversely proportional to frequency, which is wrong [23]. To solve such a breakdown problem originated from the right-hand side of the EFIE, we develop the following analytical method that is valid at all frequencies.

We rewrite the incident plane wave as the following:

$$\mathbf{E}_i = \hat{E}_0 + \hat{E}_0(e^{-j\mathbf{k}\cdot\mathbf{r}} - 1). \tag{29}$$

Since $\hat{E}_0$ has no space dependence, it is curl free. We hence can represent it as a gradient field. With (29), the $\mathbf{W}_0^T V$ term in (27) can be rewritten as

$$\mathbf{W}_0^T V = \mathbf{W}_0^T(V_1 + V_2) \tag{30}$$

where

$$\begin{aligned} V_{1,m} &= \iint_{S_m} \mathbf{J}_m(\mathbf{r})\cdot\hat{E}_0 dS, \\ V_{2,m} &= \iint_{S_m} \mathbf{J}_m(\mathbf{r})\cdot\hat{E}_0(e^{-j\mathbf{k}\cdot\mathbf{r}} - 1)dS. \end{aligned} \tag{31}$$

Since $\mathbf{W}_0$ represents a divergence-free current, which can be written as $\nabla\times(\psi\hat{n})$ and hence $\hat{n}\times\nabla\psi$ [3] with ψ being a scalar, its inner product with a gradient field can be analytically proved to be zero. As a result, $\mathbf{W}_0^T V_1 = 0$, (30) becomes

$$\mathbf{W}_0^T V = \mathbf{W}_0^T V_2. \tag{32}$$

If we do not utilize the analytical property of $\mathbf{W}_0^T V_1 = 0$ to vanish the V_1 term in (30), at low frequencies where V_2 becomes negligible, (30) will be dominated by $\mathbf{W}_0^T V_1$. Thus the term

$\mathbf{W}_0^T V$ will have a completely wrong frequency dependence at low frequencies.

With (32), (27) becomes

$$I_0 = \frac{1}{j\omega}\mathbf{W}_0\mathbf{W}_0^T V_2 \overset{V_2 \simeq j\omega}{\rightarrow} \text{constant}. \tag{33}$$

At very low frequencies, V_2 scales linearly with frequency as can be seen from (31). Hence, the divergence-free current I_0 for an incident plane wave excitation is a constant that does not change with frequency, which agrees with low-frequency electromagnetic field theory [23]. As for the nonsolenoidal component of the current, from (28), we obtain

$$I_h = j\omega\mathbf{W}_h(\Lambda_h)^{-1}\mathbf{W}_h^T V \tag{34}$$

at low frequencies, which also agrees with the low-frequency electromagnetic theory as it represents the current associated with a charge having a constant magnitude, and hence scaling with frequency linearly.

Since the inner product between a divergence-free current and a gradient field is zero irrespective of frequency, the treatment used in (32) is universal in the sense it is valid for all frequencies. Hence, in (26) that is true for all frequencies, the $\mathbf{W}_0^T V$ term can be corrected in the same way. As for the evaluation of $\mathbf{W}_h^T V$, no special treatment is required.

2) Solution to the Delta-Gap Source-Based Right-Hand Side V: In many applications such as circuit extraction and antenna impedance calculation, the right-hand side V used is a delta-gap voltage source. In this case, the frequency dependence of I_0 and I_h can be readily recognized from (26), which is given below

$$I = I_0 + I_h = \frac{1}{j\omega}\mathbf{W}_0\mathbf{W}_0^T V + j\omega\mathbf{W}_h(\Lambda_h)^{-1}\mathbf{W}_h^T V. \tag{35}$$

Unlike the plane-wave incident case where I_0 is real and I_h is imaginary at low frequencies, both I_0 and I_h are imaginary. Furthermore, I_0 is inversely proportional to frequency, while I_h scales with frequency linearly. This reveals that I_0 represents the current through an inductor, while the I_h is the current through a capacitor, and the circuit model of (35) is a constant V source applied to an inductor in parallel with a capacitor. In addition, the weights of the higher order eigenmodes in the current solution are proportional to $j\omega(\lambda_h - \omega^2)^{-1}$, whereas that of the dc eigenmodes scale as $1/\omega$. When inductance and capacitance co-exist, although the current through the capacitance, I_h, can be negligible as compared with the inductance current, the $\mathbf{E}$ field generated by the I_h is important at low frequencies. This will become clear from the following subsection.

C. Scattered Field and RCS Computation From Zero to High Frequencies

The computation of scattered fields including both near and far fields also breaks down at low frequencies if not done correctly. In this section, we present an analytical method to overcome this breakdown. This method is valid at all frequencies.

The scattered $\mathbf{E}$ field, $\mathbf{E}^{\text{sca}}(\mathbf{r})$, can be computed from the current $\mathbf{J}$ as the following:

$$\mathbf{E}^{\text{sca}}(\mathbf{r}) = \iint_S [j\omega\mu\mathbf{J}(\mathbf{r}')G(\mathbf{r},\mathbf{r}') + \frac{1}{j\omega\varepsilon}(\nabla'\cdot\mathbf{J}(\mathbf{r}')\nabla' G(\mathbf{r},\mathbf{r}')]dS. \tag{36}$$

The RCS is defined as

$$\text{RCS} = \lim_{r\to\infty} 4\pi r^2 \frac{|\mathbf{E}^{\text{sca}}(\mathbf{r})|^2}{|\mathbf{E}^{\text{inc}}|^2} \tag{37}$$

where, in far field analysis, we consider θ- and φ-components of the $\mathbf{E}^{\text{sca}}(\mathbf{r})$. The two components are contributed only by the first term of (36), which is associated with the vector potential and can be evaluated for the far field as

$$\begin{aligned} j\omega\mathbf{A}_{\text{far}}(\mathbf{r}) &= \iint_S [j\omega\mu\mathbf{J}(\mathbf{r}')G(\mathbf{r},\mathbf{r}')]dS \\ &= \frac{j\omega\mu}{4\pi r}e^{-jkr}\iint_S \mathbf{J}(\mathbf{r}')e^{jkr'\cos\psi}dS, \end{aligned} \tag{38}$$

where

$$\cos\psi = \frac{\mathbf{r}\cdot\mathbf{r}'}{rr'}. \tag{39}$$

From (25), (26), it can be seen that at any frequency that is either high or low, current $\mathbf{J}$ can be written as

$$\mathbf{J} = \tilde{\mathbf{J}}_0(\omega) + \tilde{\mathbf{J}}_h(\omega) \tag{40}$$

where $\tilde{\mathbf{J}}_0$ is the divergence-free current associated with $\mathbf{W}_0$, and $\tilde{\mathbf{J}}_h$ is the nonsolenoidal current associated with $\mathbf{W}_h$.

By substituting (40) into (38), we obtain for the far field

$$\begin{aligned} j\omega\mathbf{A}_{\text{far}}(\mathbf{r}) &= \iint_S [j\omega\mu\mathbf{J}(\mathbf{r}')G(\mathbf{r},\mathbf{r}')]\, dS \\ &= \frac{j\omega\mu}{4\pi r}e^{-jkr}\iint_S \tilde{\mathbf{J}}_0 e^{jkr'\cos\psi}\, dS \\ &\quad + \frac{j\omega\mu}{4\pi r}e^{-jkr}\iint_S \tilde{\mathbf{J}}_h e^{jkr'\cos\psi}\, dS. \end{aligned} \tag{41}$$

In the above, the computation of the first term breaks down at low frequencies. This is because, due to finite machine precision, the correct frequency dependence of the first term will be lost when $e^{jkr'\cos\psi}$ is treated as 1 in computation at low frequencies. To fix this problem, again, like the approach we developed to fix the low-frequency breakdown of $\mathbf{W}_0^T V$ in Section III-B, we split $e^{jkr'\cos\psi}$ into 1 and $e^{jkr'\cos\psi} - 1$. We then analytically vanish the gradient-field related component of $e^{jkr'\cos\psi}$, which is 1, because the inner product of the divergence-free current $\tilde{\mathbf{J}}_0$ and a gradient field is analytically known to be zero. Thus, (41) is corrected to be

$$\begin{aligned} j\omega\mathbf{A}_{\text{far}}(\mathbf{r}) &= \iint_S [j\omega\mu\mathbf{J}(\mathbf{r}')G(\mathbf{r},\mathbf{r}')]dS \\ &\rightarrow \frac{j\omega\mu}{4\pi r}e^{-jkr}\iint_S \tilde{\mathbf{J}}_0(e^{jkr'\cos\psi} - 1)dS \\ &\quad + \frac{j\omega\mu}{4\pi r}e^{-jkr}\iint_S \tilde{\mathbf{J}}_h e^{jkr'\cos\psi}dS. \end{aligned} \tag{42}$$

As a result, the low-frequency breakdown of the first-term in (41) is fixed analytically. Moreover, (42) is true at high frequencies also. Thus, one can use it to obtain correct RCS at any frequency. The $\tilde{\mathbf{J}}_0$ and $\tilde{\mathbf{J}}_h$ in (42) can be evaluated from (26), with $\mathbf{W}_0^T V$ therein evaluated based on (31), without making any approximation.

From (42), we can also analyze the frequency dependence of $\mathbf{E}^{\text{sca}}(\mathbf{r})$ at low frequencies. Since at low frequencies, $\tilde{\mathbf{J}}_0$ is a constant as can be seen from (33), while $\tilde{\mathbf{J}}_h$ scales linearly with frequency as shown in (34), both terms in (42) scale with frequency quadratically. Note that $(e^{jkr'\cos\psi} - 1)$ in the first

term of (42) scales with frequency linearly at low frequencies since it becomes a sin function of frequency. In other words, the scattered field generated by both the divergence-free current and the nonsolenoidal current scales quadratially with frequency at low frequencies, and at dc, the scattered field in the far field is zero.

The aforementioned approach is equally applicable to the computation in the near fields or at any point that is not far. In this case, both terms in (36) are present. By substituting (40) into (36), we obtain

$$\mathbf{E}^{\mathrm{sca}}(\mathbf{r}) = \iint_S j\omega\mu \left[\tilde{\mathbf{J}}_0 + \tilde{\mathbf{J}}_h\right] \frac{e^{-jk|\mathbf{r}-\mathbf{r}'|}}{4\pi|\mathbf{r}-\mathbf{r}'|} dS + \iint_S \frac{1}{j\omega\varepsilon} (\nabla' \cdot \tilde{\mathbf{J}}_h(\mathbf{r}')\nabla' G(\mathbf{r},\mathbf{r}') dS \quad (43)$$

where the divergence of $\tilde{\mathbf{J}}_0$ is analytically vanished in the second term. In the above, the computation of the first term breaks down at low frequencies. Again, to fix it, we split $e^{jk|\mathbf{r}-\mathbf{r}'|}$ into 1 and $e^{jk|\mathbf{r}-\mathbf{r}'|} - 1$. Equation (43) can then be written as

$$\mathbf{E}^{\mathrm{sca}}(\mathbf{r}) = \iint_S j\omega\mu\tilde{\mathbf{J}}_0 \frac{(e^{-jk|\mathbf{r}-\mathbf{r}'|} - 1)}{4\pi|\mathbf{r}-\mathbf{r}'|} dS + \iint_S j\omega\mu\tilde{\mathbf{J}}_h \frac{e^{-jk|\mathbf{r}-\mathbf{r}'|}}{4\pi|\mathbf{r}-\mathbf{r}'|} dS + \iint_S \frac{1}{j\omega\varepsilon} (\nabla' \cdot \tilde{\mathbf{J}}_h(\mathbf{r}')\nabla' G(\mathbf{r},\mathbf{r}') dS \quad (44)$$

which no longer breaks down at low frequencies, and is valid at any frequency. At zero frequency, only the last term is left, which is nothing but the gradient field generated by constant charges [notice that $\tilde{\mathbf{J}}_h$ obtained from the proposed method scales linearly with frequency as shown in (34)]. Equation (44) is equally applicable to the total field calculation for the frequency-independent right-hand side V. As can be seen from (35), although in this case $\tilde{\mathbf{J}}_h$ is negligible as compared with $\tilde{\mathbf{J}}_0$ at low frequencies, the $\mathbf{E}$ field generated by $\tilde{\mathbf{J}}_h$ is dominant.

IV. Answers to Theoretical Questions Related to Low-Frequency Breakdown

The solution proposed in the previous section provides a rigorous solution to the original fullwave system of equations of the EFIE at any frequency. With this solution known, we can provide decisive answers to a few important theoretical questions relating to the low-frequency breakdown. To make our explanation clear, in Fig. 1, we plot an axis of the absolute eigenvalues of (8), along which we illustrate the relative relationship between zero eigenvalues 0, the square of the highest breakdown frequency $\omega^2_{\mathrm{break}}$, the smallest modulus of the nonzero eigenvalues of (8), λ_{h1}, and the largest modulus of the eigenvalues of (8), $\lambda_{\max}$. The distances labeled by n, m, and q are the ratios of the corresponding nonzero eigenvalues in log scale. In double-precision computing, ω_{break} can be determined based on

$$\omega^2_{\mathrm{break}} \leq 10^{-16}\rho(\mathbf{A}^{-1}\mathbf{\Phi}) = 10^{-16}\lambda_{\max}$$

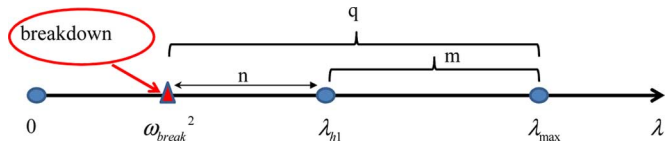

Fig. 1. Illustration of the relative relationship between $0, \omega^2_{\mathrm{break}}$, and λ_{h1}, and $\lambda_{\max}$.

where $\rho(\cdot)$ denotes the spectral radius of a matrix, which is the modulus of the largest eigenvalue of the matrix. This is because at this frequency the contribution of $\mathbf{A}$ starts to be neglected due to finite machine precision. As a result, in Fig. 1, $q = 16$ in double-precision computation. The ratio of $\lambda_{\max}$ to λ_{h1} is proportional to the square of the largest physical dimension over the smallest feature size present in the structure.

A. Dense Discretization Breakdown Versus Breakdown Due to Low Frequencies

Fig. 1 can be used to understand the similarity and difference between the breakdown due to dense discretizations and that caused by low frequencies. For a given structure, if one fixes the mesh, the eigenvalue distribution is determined, and thereby $\lambda_{\max}$ and λ_{h1}. When frequency decreases such that the ratio of ω^2 to $\lambda_{\max}$ is beyond machine precision (10^{16} in double-precision computation), breakdown starts to occur. For a given structure, if one fixes the frequency, but keeps refining the mesh, $\lambda_{\max}$ will be pushed higher and higher along the axis. This is because the square root of $\lambda_{\max}$ represents the largest complex resonance frequency at the given frequency, which is inversely proportional to the smallest mesh size. The ratio of ω^2 to $\lambda_{\max}$ hence will become smaller and smaller. Again, once this ratio is beyond machine precision, breakdown occurs. So for both cases, when the electric size square of the smallest mesh size is less than machine precision, breakdown occurs.

B. At Which Frequency Fullwave Effects Become Important?

From (20), it can be seen clearly that the weight of a higher order mode having eigenvalue λ_h in the EFIE solution is proportional to $\omega/(\lambda_h - \omega^2)$; and the weight of the dc mode in the EFIE solution is proportional to $1/\omega$. The former over the latter is $(1)/((\lambda_h/\omega^2) - 1)$. Given an arbitrary 3-D structure, if the ratio between ω^2 and the first nonzero eigenvalue λ_{h1} is less than two orders of magnitude, then fullwave effects become important since at this frequency the contribution of higher order modes in the field solution cannot be neglected for achieving an accuracy higher than 1%. The λ_{h1} (having the same unit as ω^2) can be analytically estimated from the first nonzero complex resonance frequency being simulated, which corresponds to the largest physical dimension of the structure.

C. Is Solution at the EFIE Breakdown a Static Solution?

The breakdown of the EFIE is due to finite machine precision instead of decoupled electric and magnetic fields. The precision of today's computers is *not* low. To make the EFIE break down, $\omega^2_{\mathrm{break}}$ must be ~16 orders of magnitude smaller than $\lambda_{\max}$ in double-precision computation, while the ratio between λ_{h1} and

$\lambda_{\max}$ is much less than 16 orders of magnitude even in a structure that has a several-wavelengths difference in geometrical scales. Taking an integrated circuit system as an example, where the ratio between the largest geometrical scale and the smallest scale can be viewed as one of the largest among today's engineering systems. In this system, the ratio between the largest and the smallest feature size is approximately 1 cm versus 10 nm, which is 10^6. Thus, the ratio of $\lambda_{\max}$ to λ_{h1} is 10^{12}. Therefore, in Fig. 1, $m = 12$, and hence $n > 2$ since $q = 16$ in double-precision computation. As a result, the contribution of higher order modes in the EFIE solution at breakdown is negligible, and hence the solution is dominated by static physics.

However, in applications where the ratio between λ_{h1} and $\lambda_{\max}$ is pushed close to machine precision such as problems with dense discretizations or multiscale applications that cover a more than six orders of magnitude in the ratio of geometrical scales, then ω^2_{break} becomes close to λ_{h1}, and hence when the EFIE breaks down, the higher order eigenmodes will make important contributions to the EFIE solution. As a result, there exists a range of breakdown frequencies at which the solution is dominated by fullwave effects. This theoretical prediction will be verified by a multiscale example having a seven orders of magnitude ratio in geometrical scales in the numerical result section.

V. Proposed Fast Method for Solving EFIE Breakdown

The proposed rigorous closed-form model of the EFIE's inverse shown in Section III, together with the essential idea of the proposed method for overcoming the barrier imposed by finite machine precision, can be exploited to develop a fast method to solve the EFIE breakdown without the need for solving the original generalized eigenvalue problem shown in (8). It should be noted that this method is not a fast algorithm for solving matrix equations but a fast method for solving the breakdown problem.

A. Proposed Fast Method for the Case Where the EFIE Solution at Breakdown is Dominated by Static Effects

The EFIE solution shown in (26) is true for all frequencies. In the case where the EFIE solution at breakdown frequencies is dominated by static physics, the entire structure being simulated is electrically small, as can be deduced from the analysis in Section IV-B. The matrices $\mathbf{A}$ and $\mathbf{\Phi}$ become real, and (26) is simplified to (27)–(28). The right-hand-side vector V in (27) and (28) can be either a delta-gap source or a plane wave incident field. Next, we present the proposed fast methods for both cases.

1) Case 1—Delta-Gap Source-Based Right-Hand Side: For a delta-gap source right-hand side V, it is clear that the EFIE solution is dominated by I_0, as shown in (35). It has an explicit frequency dependence. Therefore, we can use one solution vector I_{ref} obtained at a non-breakdown frequency, denoted by ω_{ref}, to obtain the EFIE solution $I(\omega)$ at any breakdown frequency as the following:

$$I(\omega) = (\omega_{\text{ref}}/\omega) I_{\text{ref}}. \tag{45}$$

The ω_{ref} can be chosen in the following band:

$$\omega^2_{\text{break}} < \omega^2_{\text{ref}} < 10^{-n}\lambda_{h1} \quad \text{with } n \geq 2 \tag{46}$$

where ω_{break} is the first breakdown frequency, and λ_{h1} is the modulus of the first nonzero eigenvalue of (8), as illustrated in Fig. 1. At such an ω^2_{ref}, the weight of the higher order modes is at least two orders of magnitude smaller than that of the dc eigenmode, and thereby negligible; and meanwhile, the EFIE solution has not yet broken down. In double-precision computing, the ω_{break} can be estimated from the following together with $\lambda_{\max}$ and λ_{h1}:

$$\omega^2_{\text{break}} \approx 10^{-16}\lambda_{\max} \quad \lambda_{\max} \sim \pi^2 c^2/l^2_{\min} \quad \lambda_{h1} \sim \pi^2 c^2/l^2_{\max} \tag{47}$$

where $l_{\min}$ represents the smallest mesh size, and $l_{\max}$ is the largest physical dimension of the structure. When the breakdown solution is dominated by static effects, the electric size corresponding to the largest physical size is small too. Therefore, the m shown in Fig. 1 is much less than 16 in double-precision computation. As a result, the range defined by (46) is fairly large. Hence, it is not difficult to select ω_{ref}. To apply an iterative solver that requires a good condition number, one can select, in the range of (46), a frequency that meets such a requirement to generate the reference solution.

For capacitor structures where physical loop currents do not exist, i.e., currents cannot form a loop physically; only I_h of (35) is of physical interest. Since I_h has a known frequency dependence, again, we can use the solution vector I_{ref} obtained at one non-breakdown frequency to obtain the EFIE solution $I(\omega)$ at any breakdown frequency as the following:

$$I(\omega) = (\omega/\omega_{\text{ref}}) I_{\text{ref}}. \tag{48}$$

Cost Analysis: The computational cost of the frequency scaling shown in (45) and (48) is trivial. The complexity of obtaining I_{ref} is the same as that of solving the traditional EFIE at one frequency. After I_{ref} is obtained, the solutions at all breakdown frequencies are obtained with negligible cost.

2) Case 2—Plane Wave Incidence in Scattering Analysis: For the scattering analysis in which the right-hand side V is frequency dependent, at low frequencies, the EFIE solution has both real and imaginary parts shown in (33) and (34). Neither I_0 nor I_h can be ignored as I_0 appears in the real part, and I_h appears in the imaginary part. However, their frequency dependences have been explicitly revealed. Based on such a frequency dependence of the EFIE solution at low frequencies, and using just a single solution I_{ref} obtained at ω_{ref}, we can obtain the solution of the EFIE at any frequency where the EFIE breaks down as follows:

$$\text{Re}[I(\omega)] = \text{Re}[I_{\text{ref}}] \quad \text{Im}[I(\omega)] = (\omega/\omega_{\text{ref}})\text{Im}[I_{\text{ref}}]. \tag{49}$$

Cost Analysis: The cost is the same as that in previous section.

B. Proposed Fast Method for the Case Where the EFIE Solution at Breakdown Frequencies is a Full-Wave Solution

In cases, where the ω^2_{ref} satisfying (46) cannot be found, the EFIE solution is dominated by full-wave effects when the EFIE breaks down. As analyzed in Section IV-C, such a case is not frequently encountered and can only happen when the ratio between λ_{h1} and $\lambda_{\max}$ is pushed so close to machine precision, such as greater than 10^{12} in double-precision computing. For

this case, we develop a method to find the EFIE solution as follows.

Consider a breakdown frequency ω_b, we first obtain the solution of (3), with the system matrix $\mathbf{Z}$ replaced by the following system matrix at a few frequencies ω where the solution does not break down:

$$\tilde{\mathbf{Z}}(\omega) = \frac{1}{j\omega}\mathbf{\Phi}(\omega_b) + j\omega\mathbf{A}(\omega_b). \tag{50}$$

Denoting the union of these solutions to the above $\tilde{\mathbf{Z}}(\omega)$ by $\mathbf{X}$, which is of size N by p, where p is the number of frequencies simulated. It is clear that the solutions in $\mathbf{X}$ and the solution at breakdown frequency ω_b being pursued are the superposition of the same set of eigenvectors since they share the same governing generalized eigenvalue problem in common. We then orthogonalize $\mathbf{X}$ to obtain $\mathbf{X}_{\rm orth}$, the size of which is N by k. With $\mathbf{X}_{\rm orth}$, we transform (8) at ω_b to a reduced eigenvalue problem

$$\mathbf{\Phi}_r(\omega_b)x = \lambda\mathbf{A}_r(\omega_b)x \tag{51}$$

where $\mathbf{\Phi}_r = \mathbf{X}_{\rm orth}^T\mathbf{\Phi}(\omega_b)\mathbf{X}_{\rm orth}, \mathbf{A}_r = \mathbf{X}_{\rm orth}^T\mathbf{A}(\omega_b)\mathbf{X}_{\rm orth}$, both of which are of size k by k. After solving the above, we obtain k eigenvectors and eigenvalues. Let the matrix of the k eigenvectors be $\mathbf{W}_r$, the eigenvectors of (8), $\mathbf{W}$, can be obtained as $\mathbf{X}_{\rm orth}\mathbf{W}_r$. This includes both dc eigenmodes (divergence-free components) denoted by $I_{\rm ref_0}$, and a few high-order eigenmodes denoted by $I_{\rm refh}$. The union of $I_{\rm ref_0}$ and $I_{\rm refh}$ can then be used as the reduced space of $O(1)$ to find the EFIE solution at ω_b. Using it, (4) becomes

$$[I_{\rm ref_0}, I_{\rm refh}]^T(\mathbf{\Phi}(\omega_b) - \omega_b^2\mathbf{A}(\omega_b))[I_{\rm ref_0}, I_{\rm refh}]y = [I_{\rm ref_0}, I_{\rm refh}]^T j\omega V(\omega). \tag{52}$$

We then fix the low-frequency breakdown in the above reduced system of $O(1)$ by analytically vanishing $\mathbf{\Phi}(\omega_b)I_{\rm ref_0}$ and $I_{\rm ref_0}^T\mathbf{\Phi}(\omega_b)$.

Again, there are two different kinds of V: one is frequency dependent, the other is frequency independent. For frequency-independent V, the computation of $I_{\rm ref_0}^T V(\omega)$ in (52) can be performed as it is without low-frequency breakdown. For frequency-dependent V encountered in the scattering analysis, the computation of $I_{\rm ref_0}^T V(\omega)$ follows the same method described in Section III-B.1 to avoid the low-frequency breakdown. Specifically, since $I_{\rm ref_0}$ is the nullspace of $\mathbf{\Phi}(\omega_b)$ representing a loop current, $I_{\rm ref_0}^T V(\omega)$ is computed like (32).

As for the choice of frequencies used for simulating (50) to build $\mathbf{X}$, these can be chosen above $\omega_{\rm break}$ and progressively added until the repeating high-order eigenvalues found from (51) are beyond the range that makes a nontrivial contribution to the solution at the simulation frequency. This is based on the fact that the relative weight of a higher order mode having eigenvalue λ_h in the EFIE solution is proportional to $1/(\lambda_h - \omega^2)$.

Cost Analysis: We analyze the cost of the proposed method step by step. 1) Solving (3) using (50) at p non-breakdown frequencies is the same as performing the traditional EFIE computation at p frequencies, where p is $O(1)$. As shown in Fig. 1, there are no additional eigenvalues between λ_{h1} and 0, therefore, the number of modes that are important for the EFIE solution at breakdown is bounded by a constant. 2) Generating the reduced matrices shown in (51) has the same complexity as performing the EFIE-based matrix-vector multiplications k times, where k is $O(1)$. 3) Solving the reduced eigenvalue problem (51) takes negligible time because of its $O(1)$ size. 4) Generating the reduced matrix in the left-hand side of (52) again has the same complexity as k-times matrix-vector multiplications, while solving (52) is trivial because of its $O(1)$ size. Overall, the total cost is dominated by the first step: the traditional EFIE solution of (50) at a few frequencies since the cost of the following steps is negligible as compared to the first step. As a result, like the "static" breakdown presented in previous section, for the "full-wave" breakdown case considered here, the proposed method can also be used to solve the EFIE breakdown with great ease.

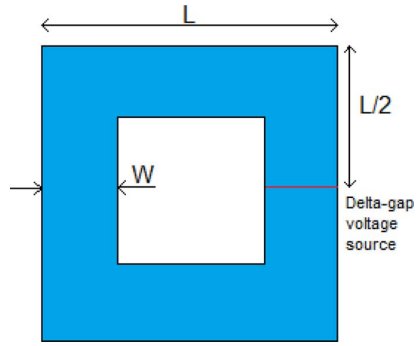

Fig. 2. Geometry of a ring inductor.

VI. Numerical Results

The accuracy and efficiency of the proposed methods have been validated by a number of circuit and scattering examples. We give four examples as follows.

A. Ring Inductor

The first example is a ring inductor, the geometry of which is shown in Fig. 2, where L is 1 μm, and W is 0.25 μm. A delta-gap voltage source is applied across one edge of the triangular element based discretization of the inductor, as illustrated in Fig. 2. For this example, the traditional RWG-based EFIE solver breaks down in the range of $10^7 - 10^8$ Hz. With the proposed method, we are able to extract a correct inductance at any low frequency, which agrees very well with the analytical result of 1.1443 pH [24], as can be seen from Table I. Three methods are compared in Table I from dc to 50 GHz: the proposed method, the proposed method without correcting the inaccurate zero eigenvalues, and the traditional RWG-based MoM solution of the EFIE. Clearly, the proposed method produces a correct inductance, whereas the traditional method and the proposed method with inexact zero eigenvalues both fail at low frequencies. For this example, the inductance is shown to be a constant across the whole range from 0 to 50 GHz because of the small physical dimension of the structure. At 50 GHz, the electric size is 1.7×10^{-4} wavelengths; while at 10^{-32} Hz, the electric size is 3.3×10^{-47} wavelengths.

In addition, for this example, we list the first 12 eigenvalues of (8) computed at 10^{-16} Hz in Table II. The first eigenvalue in Table II appears to be a very large number, however, it is, in fact, zero because there exists a greater than 16 orders of magnitude difference between the first eigenvalue (smallest one) and

TABLE I
COMPARISON BETWEEN INDUCTANCES (H) CALCULATED BY THREE METHODS

Freq (Hz)	Traditional solver	Proposed method with inexact zero eigenvalues	Proposed method
50×10^{9}	1.1452e-012	1.1452e-012	1.1452e-012
30×10^{9}	1.1452e-012	1.1452e-012	1.1452e-012
10^{9}	1.1452e-012	1.1452e-012	1.1452e-012
10^{8}	1.1453e-012	1.1357e-012	1.1452e-012
10^{7}	1.1078e-012	1.9902e-012	1.1452e-012
10^{6}	-7.1783e-012	-1.7473e-010	1.1452e-012
10^{5}	1.9878e-010	5.1647e-010	1.1452e-012
10^{4}	-1.8377e-007	5.7346e-007	1.1452e-012
10^{3}	-1.1309e-006	-2.6692e-005	1.1452e-012
10^{2}	-0.0017	-0.0107	1.1452e-012
10^{1}	0.0109	-0.4428	1.1452e-012
1	3.4740	-51.9957	1.1452e-012
10^{-16}	2.3468e+032	-7.3231e+033	1.1452e-012
10^{-32}	2.3487e+063	1.3046e+066	1.1452e-012
0	NA	NA	1.1452e-012

TABLE II
FIRST 12 EIGENVALUES ($\mathrm{rad}^2/\mathrm{s}^2$) OF THE RING INDUCTOR AT 10^{-16} Hz

1	-1.32110e+14 - 7.73653e-15 j
2	3.14588e+29 + 0.17013 j
3	3.24189e+29 + 0.169697 j
4	1.17672e+30 + 9.03492 j
5	1.71990e+30 + 3.07316 j
6	2.67712e+30 + 0.07984 j
7	2.76548e+30 + 0.07484 j
8	3.47419e+30 + 7.30378e-05 j
9	5.59809e+30 + 3.92256e-05 j
10	5.83729e+30 + 0.29044 j
11	5.94715e+30 + 0.25525 j
12	6.52519e+30 + 0.00056728 j

the largest one, which is $1.4191\mathrm{e}{+31}{+}0.02325\mathrm{j}$ (not shown in the table) for this example. In double-precision computing, any eigenvalue that is 16 orders of magnitude smaller than the largest cannot be computed correctly. When this inexact zero is involved in the computation at low frequencies, the frequency dependence of the EFIE solution computed is completely wrong, which is evident from the third column in Table I. From Table II, it can also be seen that there is a clear gap between nonzero eigenvalues corresponding to higher order eigenmodes and the zero eigenvalue. The large gap for this example is due to the fact that the structure being simulated is small, and hence the first nonzero eigenvalue is high. In fact, as long as the structure being simulated is finite, there exists a gap between the first nonzero eigenvalue and the zero eigenvalues.

B. Parallel Plate Capacitor

Next, a parallel plate capacitor structure is simulated. The capacitor length, width, and height, are set to be 5, 4, and 0.5 mm, respectively. The discretization results in 107 unknowns. A delta-gap voltage source is applied in the middle of the post between the plates. The width of the post is 0.8 mm as shown in Fig. 3. The simulation based on a conventional RWG-based EFIE solver breaks down at 1 KHz, where the 2-norm condition number of the EFIE system matrix, which

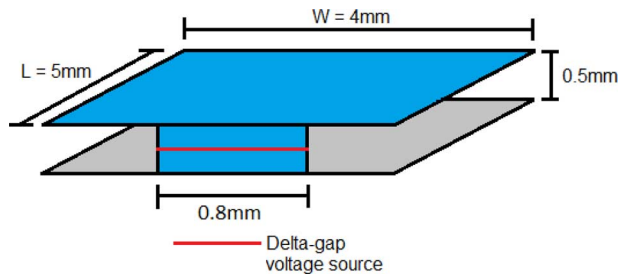

Fig. 3. Geometry of a parallel plate capacitor.

is the ratio of the largest singular value to the smallest one, is found to be $4.1131\mathrm{e}{+17}$. In contrast, the proposed solutions are valid at all frequencies. We extract the capacitance by the proposed rigorous solution at $10^5, 10^4, 10^3$, 100, 10, 1, and all the way down to 10^{-32} Hz, the capacitance obtained from the I_h part of (35) is found to be 0.459 pF. This result agrees with the traditional EFIE solution at 10^4 Hz, when the system matrix is not singular yet.

The proposed fast method is also used to simulate this example, where the solution of the EFIE at all the breakdown frequencies is obtained by a simple scaling as shown in (48). The relative difference between the solution from the proposed fast method and that of the rigorous method is found to be less than 10^{-7} across all frequencies. The reference frequency $\omega_{\mathrm{ref}}/(2\pi)$ used is 100 MHz, where the condition number of the EFIE system matrix $\mathbf{Z}$ is $5.0428\mathrm{e}{+6}$. Since there exists a wide band to select the reference frequency in a single-scaled problem or problems with a small difference in geometrical scales, one can also choose the reference frequency at 1 GHz for this example, where the condition number is $5.0424\mathrm{e}{+4}$.

Interestingly, when simulating a capacitor structure, one may not observe the EFIE breakdown numerically since the frequency scaling of the current would agree with that of the capacitor current when the contribution of the magnetic vector potential is lost. However, the system matrix is singular since matrix $\mathbf{\Phi}$ is singular, thus its numerical solution still breaks down.

C. Scattering From a Conducting Sphere

The third example is a PEC sphere with a radius of 1 m and illuminated by a plane wave. We compare the far-field RCS generated by the proposed method, the traditional RWG-based EFIE method, and Mie Series at 1 Hz in Fig. 4(a). Clearly, the result from the proposed method shows an excellent agreement with the result produced by Mie series, whereas the traditional method obviously breaks down. In Fig. 4(b), we compare the RCS generated by the proposed method and the conventional method at a high frequency 1 GHz, where the conventional method does not break down. The number of unknowns is 12 150. It is clear from Fig. 4(b) that the proposed method correlates very well with the conventional method, which demonstrates the validity of the proposed method at both high and low frequencies. In addition, one can use the proposed method to generate correct fields and RCS at arbitrarily low frequencies such as 10^{-32} Hz [25]. At these low frequencies, we have found that it becomes a must to correct the breakdown due to the loss

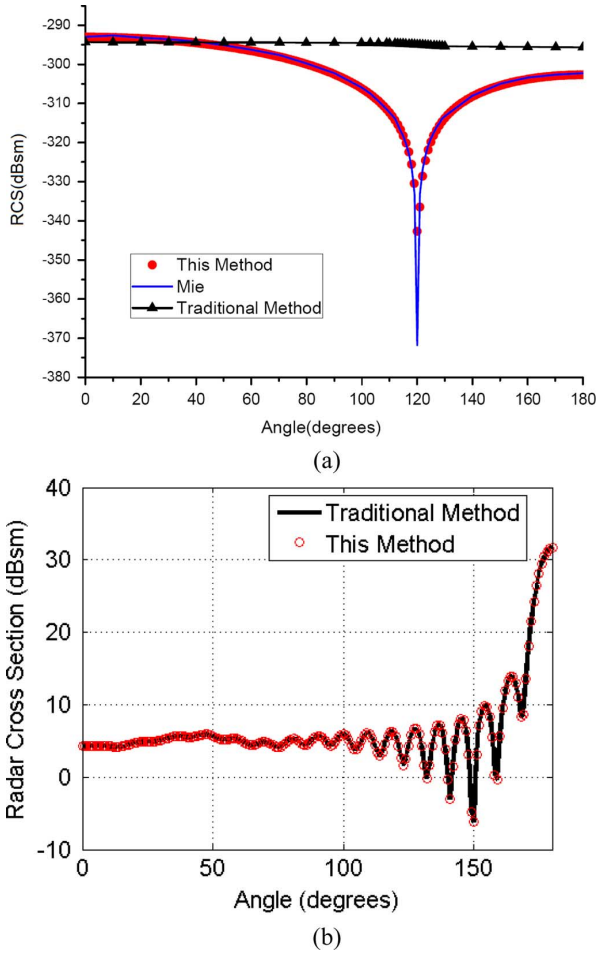

Fig. 4. Bistatic RCS comparison. (a) 1 Hz. (b) 1 GHz.

of frequency dependence in the right-hand side as well as in the scattered field calculation.

D. Multiscale Example

In the last example, we simulate a multiscaled loop inductor, the detailed geometry of which is shown in Fig. 5(a), where the width is 1 μm, the length is 1 cm, and the finest feature size is 1 nm, which is also the smallest mesh size. The two 1 nm strips shown in this figure are areas with fine discretizations. The ratio of geometrical scales spans seven orders of magnitude. There are many other multiscale examples in open literature. However, as analyzed in this paper, to observe the phenomenon that the EFIE solution at breakdown frequencies is a full-wave solution, even 3–5 orders of magnitude ratio in wavelengths would not be sufficient. That is why we designed the example shown in Fig. 5(a), the ratio of geometrical scales of which is seven orders of magnitude. The structure is excited by a delta gap voltage source applied at the horizontal edge located in the right center area, as depicted in Fig. 5.

In Table III, we list the input impedance of the multiscaled loop inductor computed from a conventional EFIE fullwave solution in comparison with the proposed method from 1 Hz to 20 GHz. From the proposed method, it can be seen that at low frequencies, the imaginary part of the input impedance scales

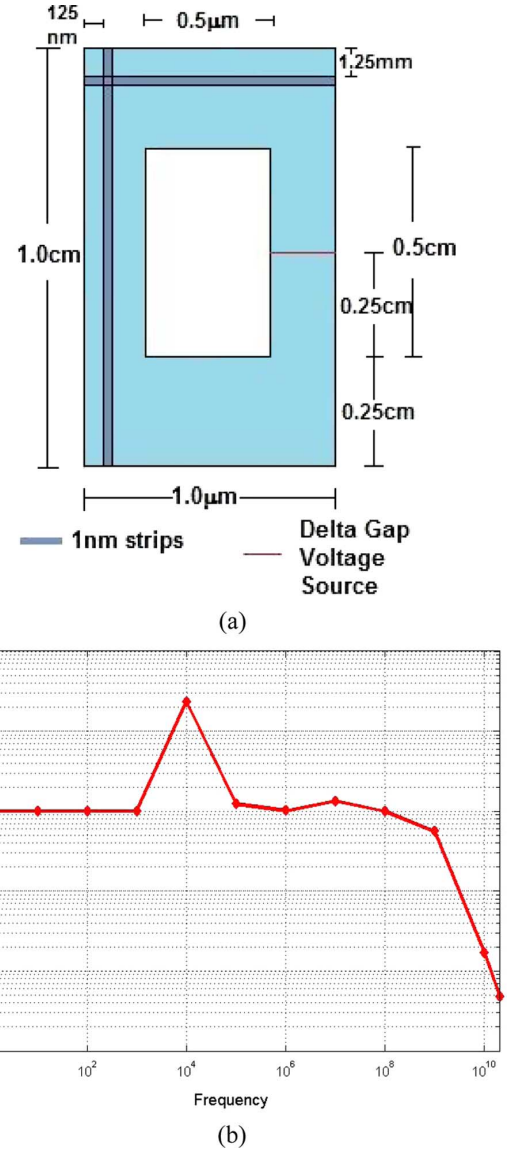

Fig. 5. Multiscaled structure. (a) Geometry (the two shaded 1 nm strips are areas with fine discretizations). (b) Solution error.

with frequency linearly, which agrees with the physical property of the structure since the structure behaves as an inductor at low frequencies. Above 1e+8 Hz, the impedance data suggests that fullwave effects start to become important. In contrast, the traditional fullwave solution fails to predict the correct frequency dependence at low frequencies. More importantly, the traditional fullwave solution breaks down even at 1 GHz, where the fullwave effects are pronounced as can be seen from the input impedance at this frequency. In Fig. 5(b), we plot the error of the entire EFIE solution of the traditional fullwave solver in comparison with the proposed solution across the entire frequency band from 1 Hz to 20 GHz, it is clear that for this multiscale example in which fine feature sizes are seven orders of magnitude smaller than the largest physical size, the breakdown occurs at frequencies where the solution is no longer a static solution. The EFIE solution error is more than 55% at 1 GHz.

In this example, we also use the proposed fast method to compute the input impedance at 1 GHz where the traditional

TABLE III
INPUT IMPEDANCE OF A MULTISCALE STRUCTURE (Ω)

Frequency (Hz)	Input Impedance (Traditional)	Input Impedance (Proposed)
1	−590386.47163 j	7.212706e-06 j
10	221.82827 j	7.212699e-05 j
1e+2	819.87776 j	0.0007212669 j
1e+3	79.31254 j	0.007212706 j
1e+4	1.137832 j	0.072127233 j
1e+5	0.136528 j	0.72126878 j
1e+6	0.999150 j	7.2126642 j
1e+7	9.980183 j	72.1265698 j
1e+8	101.85197 j	721.367481 j
1e+9	5.52702e-08+ 2297.10599 j	0.022476+ 7309.52542 j
3e+9	1.4755e-02 +1.6742e+04j	1.7315e-01 +2.4633e+04j
5e+9	1.6092e+00 +4.7974e+04j	2.4422e+00 +5.4667e+04j
7e+9	7.4302e+01 + 1.4835e+05j	1.0946e+02 + 1.8022e+05 j
1e+10	148.319564 − 77617.80553 j	139.47899− 75112.525012j
1.5e+10	1.1629e+002 − 8.0132e+003 j	1.1605e+002 − 8.0049e+003i
2e+10	2.3912e+002 +1.9373e+004 j	2.3965e+002 +1.9394e+004i

fullwave solution breaks down. We use 20 solutions uniformly sampled between 8 GHz and 15 GHz where the EFIE solution does not break down. The number of unknowns is 169. Since the EFIE solution has not broken down at these frequencies, the efficient EFIE solutions in the existing literature can all be leveraged to obtain the solutions efficiently. Robust and fast direct solutions can also be employed. These topics are not discussed here because the fast EFIE solution at *non-breakdown* frequencies is not the research problem addressed in this paper. We then solve a reduced system of $O(1)$ shown in (52) and fix the low-frequency breakdown in the reduced system. The input impedance extracted from the proposed fast method at 1 GHz is shown to be $2.68141\text{e}{-}002{+}7.3258\text{e}{+}003\text{j}$, the error of which is less than 0.2% compared to the impedance obtained from the proposed rigorous method.

VII. CONCLUSION

In this paper, the solution to the *original* full-wave EFIE system of equations is found from electrodynamic frequencies all the way down to zero frequency, thus revealing the true solution of the EFIE when it numerically breaks down due to low frequencies and/or dense discretizations. This single solution that is rigorous at all frequencies also suggests a new phenomenon that the EFIE solution at breakdown can be dominated by full-wave effects, in addition to the static solutions commonly observed when the EFIE breaks down. Such a theoretical prediction has also been verified by numerical experiments. The proposed solution of the original EFIE can also be used to find the quantitative answers to a number of theoretical questions relating to low-frequency and/or dense discretization breakdown.

The proposed closed-form expression of the EFIE's inverse, together with the essential idea of the proposed method for overcoming the EFIE breakdown, has also been exploited to develop a fast method that eliminates the EFIE breakdown efficiently. In addition, we have detailed three breakdown phenomena one can encounter in the EFIE-based low-frequency analysis, and we show how each of them is rigorously solved in this work.

It is worth mentioning that the research problem of low-frequency breakdown has certain differences from the problem of solving an ill-conditioned numerical system. The former could be solved naturally if a computer had infinite precision, while the latter could not be solved via the same means. Conversely, the latter can be well addressed by developing a well-conditioned formulation up-front, while the former, in general, cannot. This is because as long as the formulation is frequency dependent, which is true since Maxwell's equations are frequency dependent, due to finite machine precision, this formulation will inevitably lose its frequency dependence when frequency is low enough, thus breaking down or yielding inaccurate solutions. As shown in this paper, when the full-wave formulation breaks down, the solution may still be dominated by full-wave effects. Therefore, this problem can become very severe. To solve it, one would have to figure out some ways to bypass the root cause, which is the finite machine precision. This is what has been pursued and fulfilled in this paper.

Besides the EFIE, the essential idea of the proposed method is equally applicable to other integral equations and numerical methods for solving Maxwell's equations. It can also shed light on other unsolved research problems, the root cause of which is finite machine precision.

REFERENCES

[1] D. R. Wilton and A. W. Glisson, "On improving the electric field integral equation at low frequencies," in *Proc. URSI Radio Sci. Meet. Dig.*, Los Angeles, CA, USA, Jun. 1981, p. 24.
[2] J. R. Mautz and R. F. Harrington, "An E-field solution for a conducting surface small or comparable to the wavelength," *IEEE Trans. Antennas Propagat.*, vol. 32, no. 4, pp. 330–339, Apr. 1984.
[3] E. Arvas, R. F. Harrington, and J. R. Mautz, "Radiation and scattering from electrically small conducting bodies of arbitrary shape," *IEEE Trans. Antennas Propagat.*, vol. 34, no. 1, pp. 66–77, Jan. 1986.
[4] G. Vecchi, L. Matekovits, P. Pirinoli, and M. Orefice, "A numerical regularization of the EFIE for three-dimensional planar structures in layered media," *Int. J. Microw. Millimeter Wave Comput.-Aided Eng.*, vol. 7, pp. 410–431, Nov. 1997.
[5] F. P. Andriulli, K. Cools, H. Bagci, F. Olyslager, A. Buffa, S. Christiansen, and E. Michielssen, "A multiplicative Calderón preconditioner for the electric field integral equation," *IEEE Trans. Antennas Propag.*, vol. 56, pp. 2398–2412, Aug. 2008.
[6] K. Cools, F. P. Andriulli, F. Olyslager, and E. Michielssen, "Nullspaces of MFIE and Calderón preconditioned EFIE operators applied to toroidal surfaces," *IEEE Trans. Antennas Propagat.*, vol. 57, no. 10, pp. 3205–3215, Oct. 2009.
[7] M. B. Stephanson and J.-F. Lee, "Preconditioned electric field integral equation using Calderon identities and dual loop/star basis functions," *IEEE Trans. Antennas Propag.*, vol. 57, no. 4, Apr. 2009.
[8] S. Yan, J.-M. Jin, and Z. Nie, "EFIE analysis of low-frequency problems with loop-star decomposition and Calderón multiplicative preconditioner," *IEEE Trans. Antennas Propag.*, vol. 58, no. 3, pp. 857–867, Mar. 2010.
[9] J. Zhao and W. C. Chew, "Integral equation solution of Maxwell's equations from zero frequency to microwave frequencies," *IEEE Trans. Antennas Propag.*, vol. 48, no. 10, pp. 1635–1645, Oct. 2000.
[10] F. P. Andriulli and G. Vecchi, "A Helmholtz-stable fast solution of the electric field integral equation," *IEEE Trans. Antennas Propagat.*, vol. 60, no. 5, pp. 2357–2366, May 2012.

[11] X. Y. Xiong, L. J. Jiang, W. Sha, and Y. H. Lo, "A new EFIE method based on Coulomb gauge for the low-frequency electromagnetic analysis," *PIERS*, vol. 140, pp. 613–631, Jun. 2013.
[12] M. Taskinen and P. Yla-Oijala, "Current and charge integral equation formulation," *IEEE Trans. Antennas Propag.*, vol. 54, no. 1, pp. 58–67, Jan. 2006.
[13] F. Vico, M. Ferrando-Bataller, A. Valero-Nogueira, and E. Antonino-Daviu, "A non-resonant current and charge integral equation," in *2013 7th Eur. Conf. Antennas and Propagat.*, 2013, pp. 407–410.
[14] Z. Qian and W. Chew, "Enhanced A-EFIE with perturbation method," *IEEE Trans. Antennas. Propag.*, vol. 58, no. 10, pp. 3256–3264, Oct. 2010.
[15] Z. Qian and W. Chew, "Fast full-wave surface integral equation solver for multiscale structure modeling," *IEEE Trans. Antennas Propag.*, vol. 57, no. 11, pp. 3594–3602, Nov. 2009.
[16] R. J. Adams, "Physical and analytical properties of a stabilized electric field integral equation," *IEEE Trans. Antennas Propag.*, vol. 52, no. 2, pp. 362–372, Feb. 2004.
[17] J. Zhu and D. Jiao, "A theoretically rigorous full-wave finite-element-based solution of Maxwell's equations from dc to high frequencies," *IEEE Trans. Adv. Packag.*, vol. 33, no. 4, pp. 1043–1050, Apr. 2010.
[18] J. Zhu and D. Jiao, "A rigorous solution to the low-frequency breakdown in full-wave finite-element-based analysis of general problems involving inhomogeneous lossless/lossy dielectrics and non-ideal conductors," *IEEE Trans. Microw. Theory Tech.*, vol. 59, no. 12, pp. 3294–3306, Dec. 2011.
[19] J. S. Zhao, W. C. Chew, T. J. Cui, and Y. H. Zhang, "Cancellations of surface loop basis functions," in *Proc. IEEE Antennas Propag. Symp.*, 2002, pp. 58–61.
[20] S. M. Rao, D. R. Wilton, and A. W. Glisson, "Electromagnetic scattering by surfaces of arbitrary shape," *IEEE Trans. Antennas Propag.*, vol. 30, pp. 409–418, May 1982.
[21] G. Strang, *Linear Algebra and Its Applications*, 4th ed. Independence, KY, USA: Cengage Learning, 2005.
[22] G. W. Stewart, *Matrix Algorithms, Volume II: Eigensystems*. Philadelphia, PA, USA: SIAM, 2001.
[23] R. F. Hanington, *Time Harmonic Electromagnetic Fields*. New York, NY, USA: McGraw-Hill, 1961.
[24] F. E. Terman, *Radio Engineers' Handbook*, 1st ed. London, U.K.: McGraw-Hill, 1950.
[25] S. Omar and D. Jiao, "An analytical approach to the low-frequency breakdown of the right hand side and scattered field computation in EFIE," in *Proc. IEEE Int. Symp. Antennas and Propagat.*, Jul. 2013, pp. 69–79.
[26] J. Zhu, S, Omar, W. Chai, and D. Jiao, "A rigorous solution to the low-frequency breakdown in the electric field integral equation," in *Proc. IEEE Int. Symp. Antennas and Propagat.*, Jul. 2011.

Jianfang Zhu received the B.S. degree in electronic engineering and information science from the University of Science and Technology of China, Hefei, China, in July 2006 and the Ph.D. degree in electrical engineering from Purdue University, West Lafayette, IN, USA, in August 2011.

She currently is an Analog Engineer at Intel Corporation, Hillsboro, OR, USA. She has authored one book chapter and over 30 papers in refereed journals and international conferences.

Dr. Zhu was nominated for the Dimitris N. Chorafas Foundation Award for Outstanding Ph.D. Thesis while studying at Purdue University. Her research has been recognized by the 2010 IEEE International Symposium on Antennas and Propagation Best Student Paper Finalist Award, and the 2010 IEEE TRANSACTIONS ON ADVANCED PACKAGING Best Paper Finalist Award. She is an Area Editor of the *International Journal of Electronics and Communications*.

Saad Omar (S'13) received the B.S.E.E. degree (with highest distinction) from the University of Engineering and Technology, Lahore, Pakistan, in 2009. During the course of his Ph.D. degree in electrical and computer engineering, he also obtained the Masters in electrical and computer engineering.

Since then, he has been working as a Research Assistant with Professor Dan Jiao in the On-Chip Electromagnetics Lab, Purdue University, West Lafayette, IN, USA. His current research interests include computational and applied electromagnetics, direct integral equation solvers, inverse scattering problems, fast and high-capacity numerical methods, high-performance VLSI CAD tools, high frequency VLSI circuit design and analysis, microwave and millimeter wave circuits, and bio-electromagnetics.

Dr. Omar received the IEEE Antennas and Propagation Society Doctoral Research Award for 2013–14. His research has also been recognized by the 2014 IEEE International Symposium on Antennas and Propagation Best Student Paper Finalist Award and the 2014 IEEE International Microwave Symposium Best Student Paper Finalist Award. He was also the recipient of Pakistan's most prestigious Presidential Award, 15 gold medals and the National Talent Scholarship for his record-breaking academic performances both in Pre-Engineering and Engineering Schools. He is an active member of the IEEE, IEEE Microwave Theory and Techniques Society, IEEE Antennas and Propagation Society. and Golden Key International Honour Society.

Dan Jiao (S'00–M'02–SM'06) received the Ph.D. degree in electrical engineering from the University of Illinois at Urbana-Champaign, Champaign, IL, USA, in 2001.

She then worked at the Technology Computer-Aided Design (CAD) Division, Intel Corporation, until September 2005, as a Senior CAD Engineer, Staff Engineer, and Senior Staff Engineer. In September 2005, she joined Purdue University, West Lafayette, IN, USA, as an Assistant Professor with the School of Electrical and Computer Engineering, where she is now a Professor. She has authored two book chapters and over 200 papers in refereed journals and international conferences. Her current research interests include computational electromagnetics, high-frequency digital, analog, mixed-signal, and RF integrated circuit (IC) design and analysis, high-performance VLSI CAD, modeling of microscale and nanoscale circuits, applied electromagnetics, fast and high-capacity numerical methods, fast time-domain analysis, scattering and antenna analysis, RF, microwave, and millimeter-wave circuits, wireless communication, and bio-electromagnetics.

Dr. Jiao has served as a reviewer for many IEEE journals and conferences. She is an Associate Editor of the IEEE TRANSACTIONS ON COMPONENTS, PACKAGING, AND MANUFACTURING TECHNOLOGY. She received the 2013 S. A. Schelkunoff Prize Paper Award of the IEEE Antennas and Propagation Society, which recognizes the Best Paper published in the IEEE TRANSACTIONS ON ANTENNAS AND PROPAGATION during the previous year. She has been named a University Faculty Scholar by Purdue University since 2013. She was among the 85 engineers selected throughout the nation for the National Academy of Engineering's 2011 US Frontiers of Engineering Symposium. She was the recipient of the 2010 Ruth and Joel Spira Outstanding Teaching Award, the 2008 National Science Foundation (NSF) CAREER Award, the 2006 Jack and Cathie Kozik Faculty Start up Award (which recognizes an outstanding new faculty member of the School of Electrical and Computer Engineering, Purdue University), a 2006 Office of Naval Research (ONR) Award under the Young Investigator Program, the 2004 Best Paper Award presented at the Intel Corporation's annual corporate-wide technology conference (Design and Test Technology Conference) for her work on generic broadband model of high-speed circuits, the 2003 Intel Corporation's Logic Technology Development (LTD) Divisional Achievement Award, the Intel Corporation's Technology CAD Divisional Achievement Award, the 2002 Intel Corporation's Components Research the Intel Hero Award (Intel-wide she was the tenth recipient), the Intel Corporation's LTD Team Quality Award, and the 2000 Raj Mittra Outstanding Research Award presented by the University of Illinois at Urbana-Champaign.